PCCP

RSC Publishing

PAPER

A kinetic and mechanistic study into the formation of the Cu–Cr layered double hydroxide†

Cite this: *Phys. Chem. Chem. Phys.*, 2013, **15**, 8616

Gareth R. Williams,*[ab] Alexander Clout[b] and Jonathan C. Burley[c]

Received 3rd December 2012,
Accepted 1st February 2013

DOI: 10.1039/c3cp44339f

www.rsc.org/pccp

The formation of the layered double hydroxide $[Cu_2Cr(OH)_6]Cl{\cdot}yH_2O$ from the reaction between CuO and aqueous $CrCl_3{\cdot}6H_2O$ was explored using synchrotron X-ray diffraction and *ex situ* analyses. The use of hard X-rays permitted time-resolved *in situ* studies to be performed as the reaction proceeded under a range of conditions. Additional information was obtained from *ex situ* experiments in which aliquots of the reaction mixture were removed, quenched, and subsequently analysed by laboratory X-ray diffraction, IR, UV-visible, and atomic emission spectroscopies. On the basis of these data, it is proposed that the reaction involves three steps. First, the solid CuO starting material is hydrolysed to give $Cu(OH)_2$ chains, releasing Cu^{2+} ions into solution. The Cu hydroxide chains subsequently condense with aqueous Cr^{3+} species, Cl^- ions and water molecules to give a hydrated form of the LDH. This material then extrudes some water to form a phase with a reduced interlayer spacing.

Introduction

Layered double hydroxides (LDHs) are a widely-studied class of ion exchange materials. Their structure comprises positively-charged layers, with anions located between these sheets to ensure overall charge neutrality. LDHs may be described by the generic formula $[M^{II}_{1-n}M^{III}_{n}(OH)_2](X^{z-})_{n/z}{\cdot}yH_2O$, where M^{II} is often one of Mg^{2+}, Ca^{2+}, Co^{2+}, Ni^{2+}, Cu^{2+}, or Zn^{2+} and M^{III} is Al^{3+}, Fe^{3+} or Cr^{3+} (*inter alia*).[1–3] Typical materials include $[Mg_2Al(OH)_6]Cl{\cdot}yH_2O$ and $[Ca_2Al(OH)_6]Cl{\cdot}yH_2O$. There also exists a family of LDHs containing Li^+ and Al^{3+}, with compositions of the form $[LiAl_2(OH)_6]X{\cdot}yH_2O$.[4,5] A wide variety of synthetic routes to LDHs is known, the most commonly used of which is the coprecipitation method. In this process a mixed metal salt solution is combined with a basic solution, and the solid LDH precipitates out from this reaction gel: a broad range of variants have been reported.[6–9] A second method exploits the direct reaction of a metal salt solution with a metal oxide or hydroxide (the "salt-oxide" route). For instance, $[LiAl_2(OH)_6]X{\cdot}H_2O$ ($LiAl_2$–X; X = Cl, Br, NO_3, *etc.*) is most easily prepared by the reaction of $Al(OH)_3$ with a concentrated solution of LiX.[10,11] In a number of cases, this methodology is successful at room temperature. This was first observed by Boehm[12] in the synthesis of $[Zn_2Cr(OH)_6]NO_3{\cdot}2H_2O$ *via* the suspension of ZnO in a Cr^{III} chloride solution. Other LDHs which may be prepared in this way include $[Cu_2Cr(OH)_6]X{\cdot}yH_2O$[13] ($Cu_2Cr$–X; X = Cl, NO_3, *etc.*) and $[Cd_3Cr(OH)_8]Cl{\cdot}yH_2O$.[14]

The Cu_2Cr–X LDH material is interesting because the Jahn–Teller distortion in the $Cu(OH)_6$ octahedral leads to corrugation of the layers, and to cation order at least locally (long-range order is suspected).[15–17] Unlike many other LDHs, which can be prepared with a range of cation compositions, this material can only be synthesised with a Cu : Cr ratio of 2 : 1. Several authors have proposed that the increased length of the axial Cu–OH bonds renders them more susceptible to chemical modification, and have exploited this to permanently graft a range of species including Cr oxometalates,[18,19] organic sulfonates,[20,21] carboxylates,[20,21] and phosphonates[21,22] to the layers. Cu_2Cr–Cl has also been explored for the preparation of spinels *via* the intercalation of metal oxalate complexes and subsequent calcination,[23] and as a host matrix for the polymerisation of sulfonates.[24,25] Thin films of Cu_2Cr–NO_3 have been shown to have promise for the photocatalytic destruction of pollutants.[26]

A number of researchers have explored the mechanisms by which LDHs form. For instance, O'Hare's group have made extensive use of *in situ* synchrotron X-ray diffraction techniques to investigative the formation of the $LiAl_2$–X materials from $Al(OH)_3$.[10,27] A range of different mechanisms were observed depending on the precise reaction conditions, the polymorph

[a] *UCL School of Pharmacy, University College London, 29-39 Brunswick Square, London, WC1N 1AX, UK. E-mail: g.williams@ucl.ac.uk; Fax: +44 (0)207 753 5942; Tel: +44 (0)207 763 5868*

[b] *School of Human Sciences, Faculty of Life Sciences and Computing, London Metropolitan University, 166-220 Holloway Road, London, N7 8DB, UK*

[c] *Laboratory of Biophysics and Surface Analysis, Boots Science Building, School of Pharmacy, University of Nottingham, University Park, Nottingham, NG7 2RD, UK*

† Electronic supplementary information (ESI) available. See DOI: 10.1039/c3cp44339f

of $Al(OH)_3$, and the nature of the anion X. In 2005, Xu and Lu studied the formation of the Mg–Al LDH from MgO and Al_2O_3.[28] These authors suggested that the initial stage of reaction involved the hydration of the metal oxides to form hydroxides, followed by the formation of $Al(OH)_4^-$ or Mg^{2+} aqua complexes (depending on pH), which then deposit on the solid metal hydroxides to form an LDH. A synchrotron study by Mitchell *et al.* indicated that the polytype of Mg–Al LDH produced was dependent on the synthesis temperature, with no long-lasting intermediate phases generated.[29] More recently, Zhang *et al.* have probed the formation of the same LDH using urea hydrolysis.[30] A formation mechanism was proposed involving three steps: the initial formation of amorphous Al-hydroxide aggregates, followed by small boehmite particles, and the uptake of Mg^{2+} and anions from solution by the latter. Jolivet and co-workers have additionally explored the formation of $[Zn_2Cr(OH)_6]Cl{\cdot}yH_2O$ by UV-visible spectroscopy and EXAFS.[31] $[Zn(OH_2)_6]^{2+}$ and oligomeric Cr^{3+} aqua complexes were found to form initially before the LDH phase is generated through the direct condensation of $[Zn(OH_2)_6]^{2+}$ and deprotonated Cr hexaaqua complexes.

The Cu_2Cr–X LDH can be prepared by both coprecipitation and salt-oxide routes. Schubert *et al.* undertook a systematic study in which they varied the reaction parameters to determine optimal conditions for the coprecipitation synthesis where X = Cl and NO_3.[32] Michalik and co-workers expanded this work further in 2004.[33] However, to date nothing is known of the mechanism by which the three-dimensional CuO is converted into a two-dimensional LDH in the salt-oxide synthesis. This reaction proceeds readily at room temperature, suggesting that there is some low-energy route by which the transformation may happen. In this paper, a detailed study of the formation of the Cu_2Cr–Cl LDH is reported. Hard, synchrotron, X-ray sources have been used to probe the temperature- and concentration-dependence of the process, and to obtain insight into the mechanism of the reaction. These studies have been coupled with *ex situ* measurements to gain additional insight into the transformations underway.

Methods

In situ time-resolved X-ray diffraction

DORIS. Beamline F3 of the DORIS synchrotron at the Deutsches Elektronen-Synchrotron (DESY; Hamburg, Germany) received white-beam X-rays over the energy range 13.5 to 65 keV. Reactions were performed in borosilicate glass vessels using the Oxford-Daresbury *in situ* reaction vessel.[34] This comprises a temperature-controlled furnace system with a stirrer attachment, allowing reactions to be performed using conditions analogous to those used in the synthetic laboratory. In a typical experiment, 0.634 g (8 mmol) of CuO was suspended in 12 mL of deionised water. To this was then added 4 mL of a 1 M solution of $CrCl_3{\cdot}6H_2O$, giving final a Cr^{3+} concentration of 0.25 M. The resultant suspension was then stirred and maintained at a desired temperature using a Eurotherm-controlled furnace system. Diffraction patterns were recorded every 60 s until changes in these patterns had ceased.

Data were then analysed using the "F3 Tool" software, supplied by DESY. In brief, reflections were identified and Gaussian functions fitted to these. The reflections were then integrated at each timepoint. All fits were inspected by eye to ensure that reflections were well modelled by the chosen function. The integrated data were subsequently converted into the extent of reaction, α, given by:

$$\alpha = I^t_{hkl}/I^{\max}_{hkl} \quad (1)$$

where I^t_{hkl} is the intensity of a reflection *hkl* at time *t*, and $I^{\max}_{hkl}$ is the maximum intensity of this reflection. α *vs.* time curves were then constructed and analysed using the Avrami–Erofe'ev model; more details are given in the results section.

Diamond. A second set of *in situ* experiments were undertaken on the Joint Engineering Environmental and Processing Beamline I12 (JEEP) of the Diamond Light Source.[35] This beamline produces a continuous spectrum of X-rays in the energy range from 50–150 keV, but for these experiments the beam was monochromated to an energy of 53 keV. Experiments were performed in the Oxford-Diamond *In Situ* Cell (ODISC), the details of which have been reported elsewhere.[36] In brief, ODISC comprises an IR-heated furnace system with a stirrer attachment, similar to the Oxford-Daresbury cell but with more rapid heating and cooling cycles possible. Reactions were performed using the same amounts of materials as for those on DORIS, but with glassy carbon tubes used in place of borosilicate glass (in order to ensure effective heat transfer). A Thales Pixium RF4343 detector was sited 2.5 m away from the reaction vessel. 4 s diffraction patterns were collected every 30 s until changes in these patterns were no longer observed.

Data were analysed using two methods. In the first, the Fit2D programme[37] was employed to convert the 2D data collected on the Pixium to 1D patterns.[38] These patterns were visualised using the Origin software (v9.0) and integrated using in-house routines (these fit a background to the data and then use Gaussian functions to model reflections and determine their areas). The data were then normalised and analysed using the Avrami–Erofe'ev model (more details are given in the Results section). The second method comprised a Principal Component Analysis (PCA) using protocols developed in previous reports.[39,40] Statistical analyses were undertaken using the "*R*" package (http://r-project.org) and the pcaMethods module.[41] PCA involves taking a number of correlated variables in a large dataset (diffracted intensity, peak position, time, *etc.* in the present case) and reducing these to a smaller number of orthogonal variables known as "principal components", or PCs. Subsequent PCs account for increasingly small amounts of variance in the dataset (*i.e.* the greatest amount of variance is accounted for by PC1, a smaller amount by PC2, and so forth).

Ex situ measurements

Synthesis. In a typical experiment, Cu(II) oxide (1.584 g; 19.9 mmol) was placed in a round bottomed flask, to which 40 mL of a 0.25 M solution of $CrCl_3{\cdot}6H_2O$ in deionised water

was added. The reaction was stirred rapidly at room temperature. At pre-determined time intervals, aliquots of 300 μL were removed and rapidly filtered for analysis. To obtain further insight into the nature of the solid material, additional reactions on the same scale as used for *in situ* work were performed, quenched after a given amount of time, and the solid product recovered for analysis.

X-ray diffraction. X-ray diffraction patterns were recorded using a Philips PW1830 instrument operating at 40 kV and 25 mA (Cu Kα radiation, λ = 1.5418 Å). Finely ground samples were mounted onto stainless steel plates for measurements. Diffracted intensity from the sample holder did not interfere with characterisation.

Scanning electron microscopy. Scanning electron microscopy was undertaken on a FEI Quanta 200F FEGSEM instrument. Samples were gold sputter-coated prior to examination, and images recorded at 5 kV.

IR spectroscopy. IR spectra were collected with the aid of a Bruker Vector 22 instrument equipped with an attenuated total reflectance (ATR) module. Data were recorded from 4000 to 650 cm^{-1} at 2 cm^{-1} resolution.

Atomic emission spectroscopy. Atomic emission spectroscopy was carried out using the microwave plasma-atomic emission spectroscopy (MP-AES) technique on an Agilent 4100 instrument. Samples were diluted to an appropriate range (10–25 ppm) prior to measurement.

UV-visible spectroscopy. UV-visible spectra were recorded using a Shimadzu UV1800 instrument between 1100 and 300 nm. Solutions were diluted to an appropriate concentration range prior to measurement.

Results

In situ studies

Temperature variation

DORIS experiments. Beamline F3 of the DORIS synchrotron is equipped with a single Ge energy-dispersive detector, which limits the range of *d*-spacings which may be simultaneously observed. Trial experiments showed that it was not possible to follow simultaneously the CuO starting material and the LDH product reflections. This means that complete information on the mechanism of the reaction could not be obtained, but by locating the detector in the optimal position to follow the growth in intensity of the product *003* reflection it proved possible to elucidate the reaction kinetics and obtain some information on mechanism.

Experiments were performed over the temperature range from 45 to 95 °C. As is intuitively expected, the reaction is observed to proceed more rapidly at elevated temperatures. There is a short induction time observed before any product forms, the length of which increases as the temperature of reaction is lowered. At temperatures above 75 °C, the reaction was complete very quickly (within *ca.* 5 minutes), and hence reliable kinetic and mechanistic parameters could not be extracted. However, at lower temperatures more detailed information could be determined. A 3D stacked plot for the reaction at 60 °C is given in Fig. 1. The reaction product has a *d*-spacing of *ca.* 7.75 Å, consistent with the literature value of 7.7 Å for the *003* reflection of the Cu_2Cr–Cl LDH material.[13,42] There also appears to be a short-lived and poorly crystalline intermediate phase with a Bragg peak at approximately 10.5 Å. In order to gain a more quantitative understanding of the reaction process, the Cu_2Cr–Cl *003* reflections were integrated, and the integrated intensities converted into α, the extent of reaction, using eqn (1). Extent of reaction *vs.* time plots are given in Fig. 2.

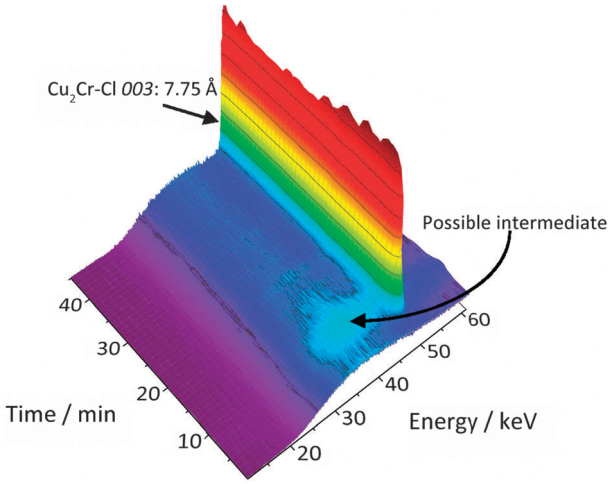

Fig. 1 3D stacked plot showing the formation of Cu_2Cr–Cl at 60 °C with 0.25 M $CrCl_3 \cdot 6H_2O$.

The Avrami–Erofe'ev model is often applied to the study of reaction processes in the solid state.[43–45] This equation takes the form:

$$\alpha = 1 - e^{-k(t-t_0)^n} \quad (2)$$

α is the extent of reaction determined from eqn (1), *n* is the reaction exponent, which contains information on mechanism, *k* is the rate constant for the process, *t* is the elapsed time, and t_0 is the induction time. The equation is found to fit the

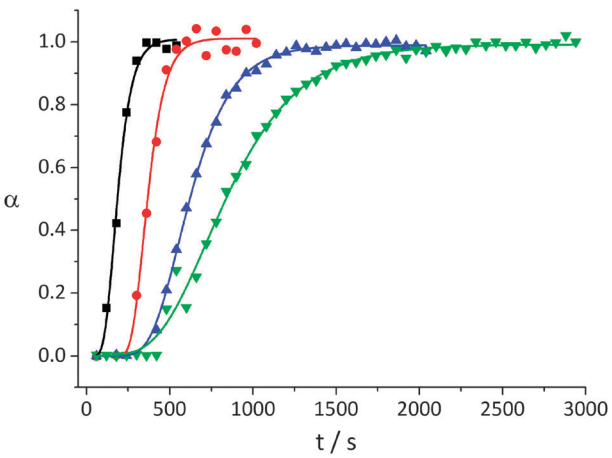

Fig. 2 Extent of reaction *vs.* time plots for the formation of Cu_2Cr–Cl with 0.25 M $CrCl_3 \cdot 6H_2O$ at (■) 70, (●) 60, (▲) 50 and (▼) 45 °C.

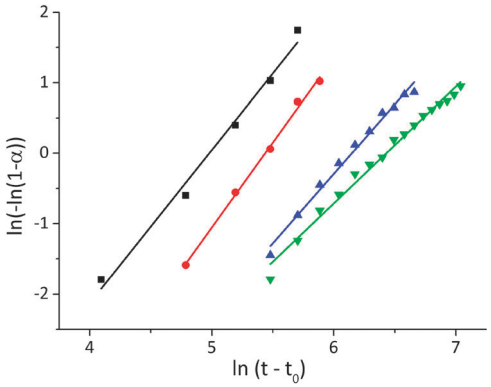

Fig. 3 Sharp–Hancock plots for the formation of Cu_2Cr–Cl with 0.25 M $CrCl_3 \cdot 6H_2O$ at (■) 70, (●) 60, (▲) 50 and (▼) 45 °C.

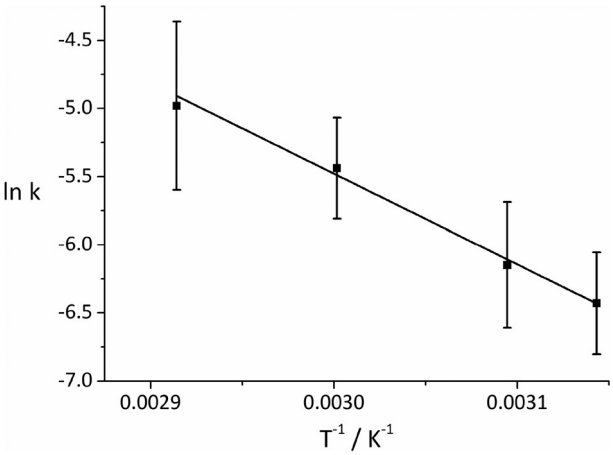

Fig. 4 Arrhenius plot for Cu_2Cr–Cl formation with 0.25 M $CrCl_3 \cdot 6H_2O$.

experimental data most closely in the range $0.15 < \alpha < 0.85$. It can be conveniently recast as the Sharp–Hancock expression, given in eqn (3).

$$\ln(-\ln(1 - \alpha)) = n \ln k + n \ln (t - t_0) \quad (3)$$

Initially in this analysis, the Avrami–Erofe'ev model (eqn (2)) was fitted directly to the extent of reaction *vs.* time data. While a good fit was observed, because the reactions were fairly rapid – leading to relatively few points in the growth curve – the errors in the parameters calculated were unacceptably high (often of the order of 50%). Therefore, the Sharp–Hancock approach to analysis was employed to analyse the data over the range $0.15 < \alpha < 0.85$, with t_0 obtained from manual inspection of the data (the values determined in this way were very similar to those calculated from Avrami–Erofe'ev fitting). The resultant plots are shown in Fig. 3 and the calculated parameters in Table 1. The Sharp–Hancock plots are observed to be highly linear ($R^2 > 0.98$), demonstrating that the Avrami–Erofe'ev model is applicable to these systems. The exponent, n, lies in the range 1.66–2.41. Hulbert has analysed the various possible reaction pathways, and proposed values of n associated with each (for some values of n more than one reaction pathway may be possible, and so a single reaction pathway might not be identifiable).[46] It appears that in this case the reaction mechanism is nucleation controlled (as $n > 0.5$). It is not possible to unambiguously determine the reaction mechanism as several are consistent with the observed values, but since $1.5 < n < 2.5$ it is postulated that 3D diffusion control following deceleratory nucleation is operational at all temperatures.

Table 1 Kinetic and mechanistic parameters determined from Sharp–Hancock analyses for the formation of Cu_2Cr–Cl at different temperatures, using a 0.25 M solution of $CrCl_3 \cdot 6H_2O$

T/°C	n	$k/10^{-3}$ s^{-1}	t_0/s	R^2
45	1.66 ± 0.05	1.61 ± 0.29	360	0.987
50	1.97 ± 0.07	2.31 ± 0.08	240	0.988
60	2.41 ± 0.08	4.35 ± 0.15	180	0.995
70	2.17 ± 0.13	6.87 ± 0.26	60	0.985

From the rate constant values, it is possible to estimate the activation energy for this process using the Arrhenius relationship. The results of this analysis are provided in Fig. 4. The activation energy E_a is estimated to be *ca.* 55 ± 6 kJ mol^{-1}. This is consistent with a nucleation controlled process – if the reaction were purely diffusion controlled, then a value closer to 15 kJ mol^{-1} (the energy barrier to the movement of molecules through the water solvent) would be expected.[47]

At room temperature (see Fig. 5) two distinct phases are observed. Initially a reflection grows in at around 10.5 Å (this will henceforth be referred to as the α-phase). This reflection then slowly declines, with concomitant increase in intensity of a peak at 7.75 Å (denoted the β-phase). After 180 min, an equilibrium mixture of the two phases is present.

Diamond experiments. To probe the reaction mechanism in more detail, experiments were also undertaken on Beamline I12 of the Diamond Light Source, where a much wider range of *d*-spacings can be simultaneously monitored. Plots of the data recorded at 50 °C and RT are shown in Fig. 6. At 50 °C (Fig. 6(a)),

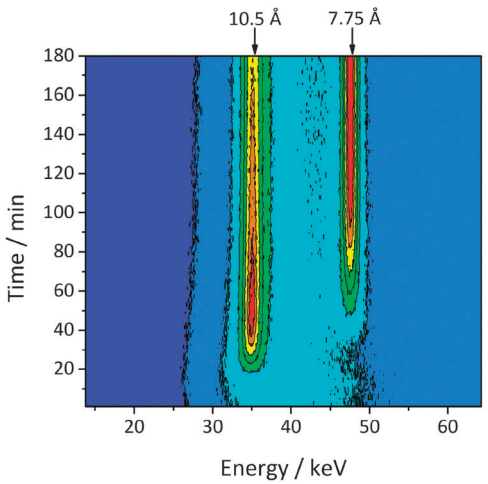

Fig. 5 Contour plot showing the reaction between CuO and a 0.25 M $CrCl_3 \cdot 6H_2O$ solution at room temperature as monitored by *in situ* EDXRD on Beamline F3.

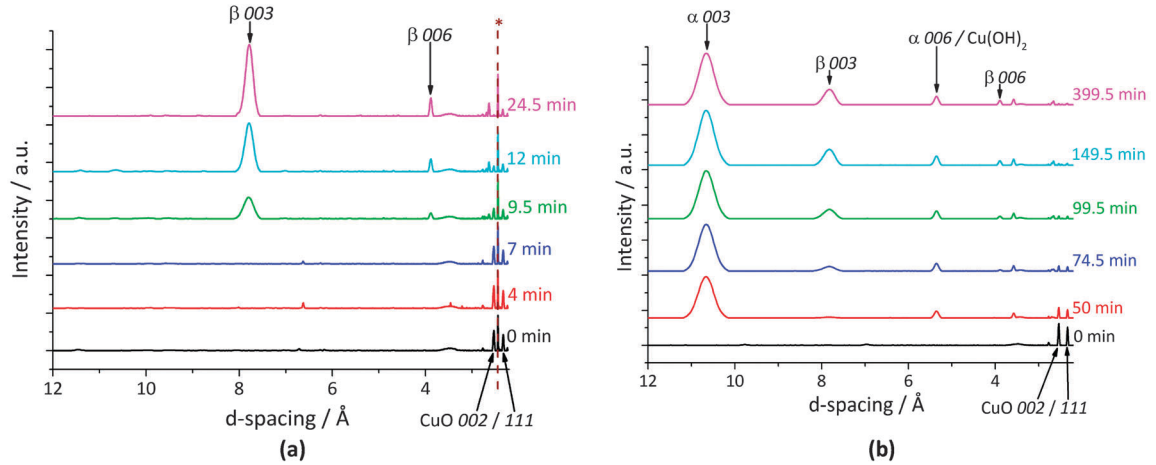

Fig. 6 Selected XRD patterns collected on Beamline I12 of the Diamond Light Source at (a) 50 °C; and, (b) room temperature. The peak marked * in (a) is an artefact from the experimental set-up.

the CuO starting material is observed to be converted directly into the Cu_2Cr–Cl product. Under these conditions, the α-phase is too transient to be seen (probably as a result of more efficient heat transfer from the furnace to the reaction solution on ODISC). At room temperature (Fig. 6(b)), the α-phase forms initially, and is then slowly converted into the β-phase. Principal component analysis of the experimental data verifies these observations: results are given in Fig. 7. At 50 °C, principal components (PC) 1 and 2 together account for 99.17% of the variance (PC1: 98.41%; PC2: 0.76%). At RT, PC1 accounts for 93.65% of the variance in the dataset, and PC2 for 6.01% (total 99.66%). At 50 °C therefore, there is only one change process underway (*i.e.* the transformation of CuO into β-Cu_2Cr–Cl); this is accounted for by PC1. At room temperature, PC1 accounts for significantly less of the variance, and PC2 is also important. This suggests that there are two change processes underway (the conversion of CuO into α-Cu_2Cr–Cl, and the subsequent conversion of the latter into β-Cu_2Cr–Cl). Hence, no intermediate is evidenced at 50 °C, and at RT the PCA results support the formation of two phases in equilibrium.

Extent of reaction *vs.* time curves are depicted in Fig. 8. Ideally, for a direct transformation between starting material and product the curves are expected to cross at $\alpha = 0.5$. At 50 °C, the α *vs.* time curves for the CuO *002* and β-Cu_2Cr–Cl phases cross at around $\alpha = 0.4$, while at room temperature, the CuO and α-Cu_2Cr–Cl curves cross at around 0.6. These values are close to 0.5, indicating that at 50 °C CuO is converted directly into β-Cu_2Cr–Cl with no long-lived intermediate phases; the crossing at $\alpha = 0.4$ could be a result of the more hydrated α-Cu_2Cr–Cl being formed very transiently *en route* to the β-material. Similarly, at

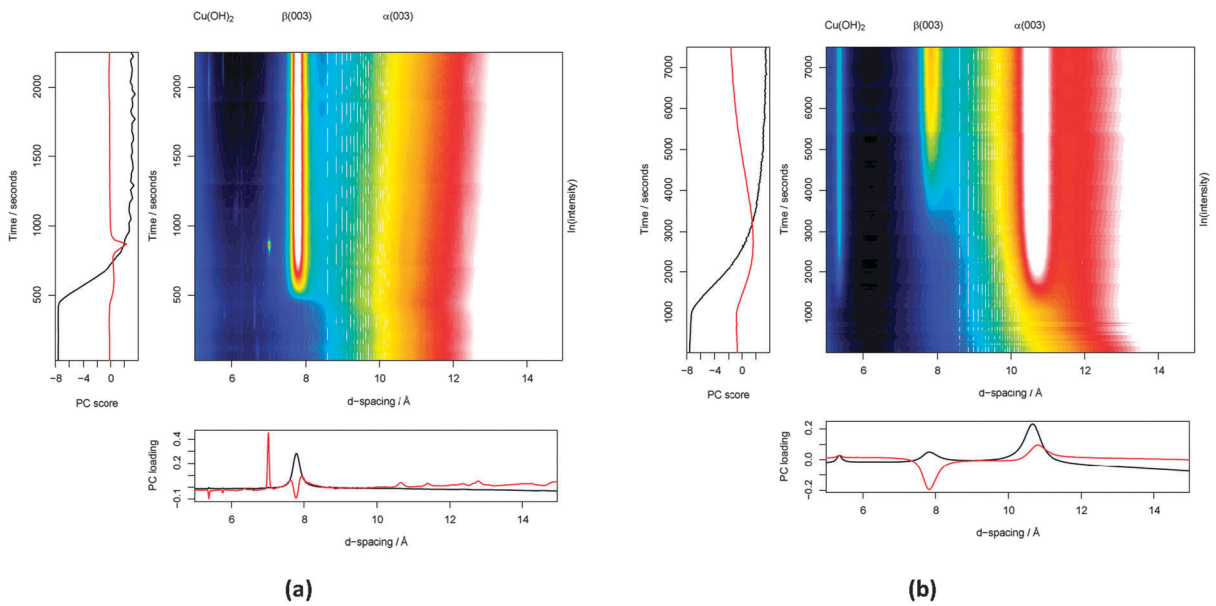

Fig. 7 PCA results for the formation of Cu_2Cr–Cl with 0.25 M $CrCl_3{\cdot}6H_2O$ at (a) 50 °C and (b) room temperature. PC1 is shown in black, and PC2 in red.

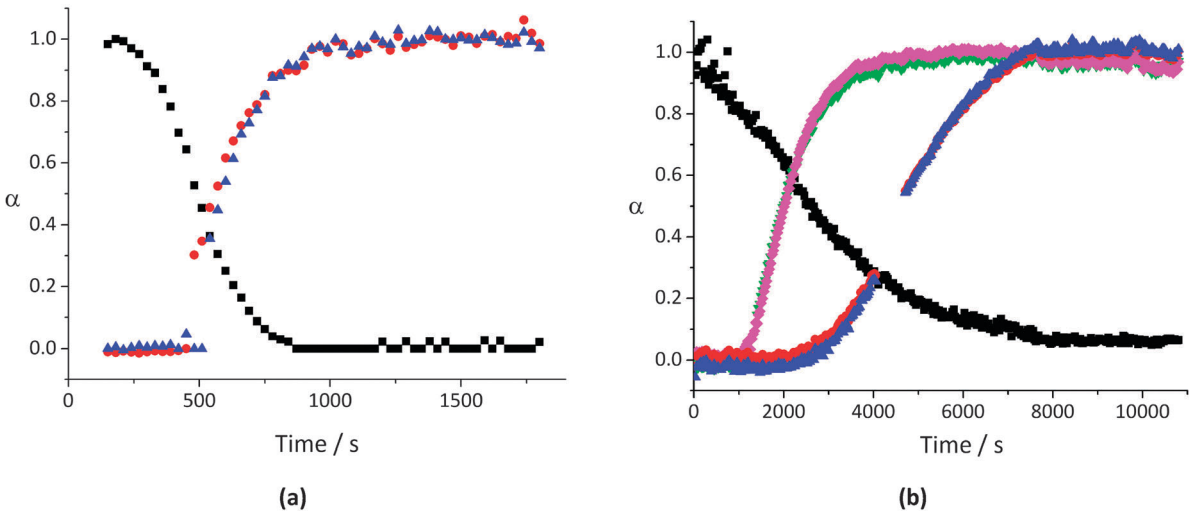

Fig. 8 Extent of reaction *vs.* time data collected on Diamond Beamline I12 for the reaction of CuO with 0.25 M $CrCl_3{\cdot}6H_2O$ at (a) 50 °C and (b) room temperature. In (a), the changing intensities of the CuO *002* (■), β-Cu_2Cr–Cl *003* (●) and *006* (▲) reflections are shown. In (b), these reflections are depicted in addition to the α-Cu_2Cr–Cl *003* (▼), and α-Cu_2Cr–Cl *006*/$Cu(OH)_2$ *020* (◆) reflections. Some points are missing from the β-Cu_2Cr–Cl growth curve in (b) owing to the integration routines not fitting the reflections satisfactorily at these time points.

RT the crossing of the starting material and α-Cu_2Cr–Cl reflections at around $\alpha = 0.6$ suggests that there is no phase lying between CuO and α-Cu_2Cr–Cl on the reaction coordinate. In contrast, at room temperature the CuO and β-Cu_2Cr–Cl curves cross at around 0.25, as a result of the β-phase forming *via* the α-material.

Concentration variation. Experiments were performed at 60 °C to study the influence of the Cr concentration on the reaction. When the final concentration of $CrCl_3{\cdot}6H_2O$ was increased beyond 0.25 M, no solid product was observed in the reaction. This is presumed to be because the low pH of the solution caused the CuO to dissolve completely. The results of reducing the $CrCl_3{\cdot}6H_2O$ concentration below 0.25 M are given in Fig. 9. The curves for solutions in the range 0.25–0.0625 M are essentially identical, with concentration having no effect on the rate of reaction. The reaction with a 0.03125 M solution has a longer induction time, but once reaction commences, the LDH forms at approximately the same rate as for the higher concentrations. The values of n determined from Sharp–Hancock plots were found to lie in the region of 1.5–2.5. The complete sets of parameters determined from Sharp–Hancock analyses are given in Table 2.

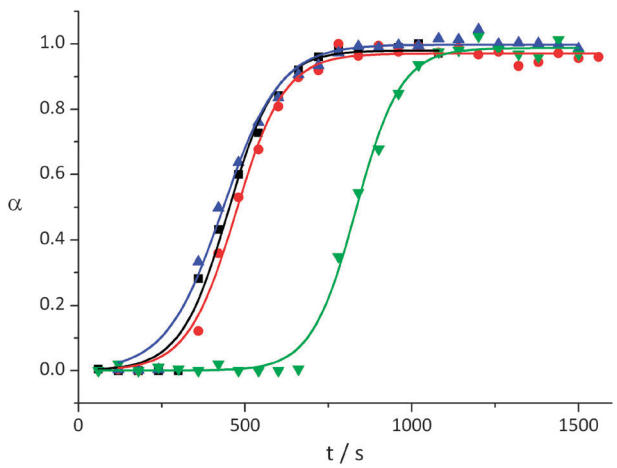

Fig. 9 Extent of reaction *vs.* time plots for the formation of Cu_2Cr–Cl in (■) 0.25, (●) 0.125, (▲) 0.0625 and (▼) 0.03125 M $CrCl_3{\cdot}6H_2O$ solutions at 60 °C.

Table 2 Kinetic and mechanistic parameters determined for the formation of Cu_2Cr–Cl at 60 °C with different concentrations of Cr chloride

$CrCl_3{\cdot}6H_2O$/M	n	$k/10^{-3}$ s^{-1}	t_0/s	R^2
0.25	2.41 ± 0.08	4.35 ± 0.15	180	0.995
0.125	1.84 ± 0.07	3.59 ± 0.17	180	0.994
0.0625	1.37 ± 0.02	3.83 ± 0.30	180	0.999
0.03125	1.57 ± 0.12	4.78 ± 0.43	660	0.982

At room temperature (see Fig. 10), two phases are observed in the system when a reduced concentration of Cr chloride is used: the β-phase and a second phase at around 5.5 Å. The latter peak cannot be the *006* reflection of the α-phase, because no peak is visible in the 10–11 Å region. There is hence a new phase existing here. Its *d*-spacing suggests that it may be $Cu(OH)_2$: this will be discussed further below. The ratio of Cu : Cr in the reaction system with 0.25 M $CrCl_3{\cdot}6H_2O$ is approximately 2 : 1: thus, with less Cr, a smaller amount of LDH can form, which may explain the observation of $Cu(OH)_2$ here.

***Ex situ* measurements.** In order to obtain more detailed information on the transformation from CuO to Cu_2Cr–Cl, a series of *ex situ* experiments were performed at room temperature. The solid products recovered through quenching were analysed by IR spectroscopy and X-ray diffraction, and the reaction solutions studied using UV-visible spectroscopy and atomic emission spectroscopy (AES).

Visual observations. Significant changes in the reaction system may be observed visually during reaction. Initially, a black solid (CuO) can be seen suspended in a green liquid. After around

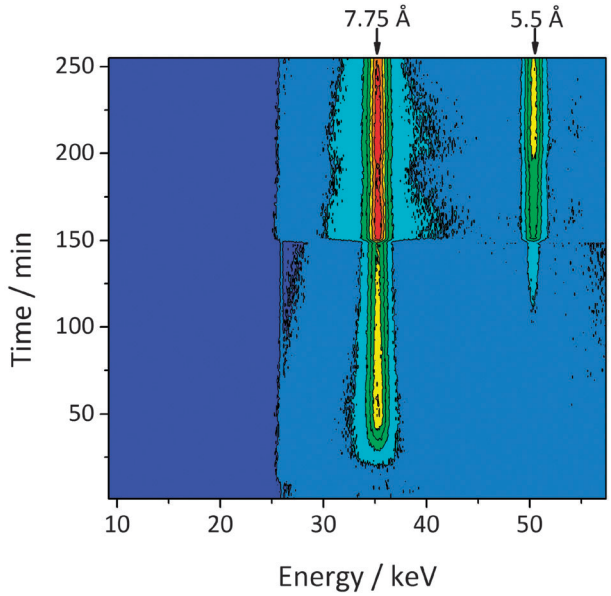

Fig. 10 Contour plot following the reaction between CuO and a 0.0625 M $CrCl_3{\cdot}6H_2O$ solution at room temperature. The discontinuity visible at *ca.* 150 min arises as a result of a beam refill taking place at this point in time.

35–45 min, the solution begins to turn rather more blue in colour. The solid products isolated after reaction times of less than 60 min are black solids, no different in physical appearance to the CuO starting material. After 70 minutes, the solid is dark brown in colour. Between 70 and 120 minutes, the colour of the solid evolves through a brown/green colour to a lighter green colour, and the solution reverts to a lighter green colour. No further colour changes are seen thereafter. The pH of the reaction system is observed to remain roughly constant at around 3.8 as these changes occur.

X-ray diffraction

Starting material and final product. The X-ray diffraction pattern of the starting material CuO could be indexed on the standard tenorite unit cell in $C2/c$,[48] with unit cell parameters a = 4.684(5) Å, b = 3.409(2) Å, c = 5.122(5) Å, and β = 99.49(14)°. The β-Cu_2Cr–Cl final product could be successfully indexed on a $R\bar{3}m$ cell with a = 3.111(1) Å and c = 23.153(7) Å, again in excellent agreement with the literature.[23,49] These X-ray diffraction patterns are included in Fig. 11.

Changes in diffraction patterns with time. As expected, in the XRD patterns of the dried products the intensities of the CuO reflections are observed to decrease with time, and those corresponding to the Cu_2Cr–Cl material grow in intensity. Sample data are shown in Fig. 12(a). The β-Cu_2Cr–Cl *003* reflection always occurs at 7.75 ± 0.1 Å and the *006* reflection at 3.85 ± 0.05 Å. The FWHM of the reflections (both from CuO and from the LDH product) are also observed to remain largely constant throughout the reaction process.

However, considering the patterns in Fig. 12(a), while the majority of reflections can be indexed to either CuO or the LDH product, there are two reflections (at 5.48 and 2.28 Å, highlighted in boxes) which do not correspond to either unit cell. These two reflections have d-spacings very close to those of $Cu(OH)_2$ (JCPDS 80-656), and first become visible after *ca.* 20–30 min of reaction. The XRD patterns of the solids isolated at intermediate time points showed diffracted intensity at approximately all d-spacings expected for $Cu(OH)_2$. A completely definitive assignment of the intermediate phase is not possible because of overlap between peaks of CuO, β-Cu_2Cr–Cl and those expected for $Cu(OH)_2$, and also because the peaks observed are at slightly higher d-spacings (by *ca.* 0.1–0.2 Å) than those predicted for $Cu(OH)_2$, but it is sensible that the reaction

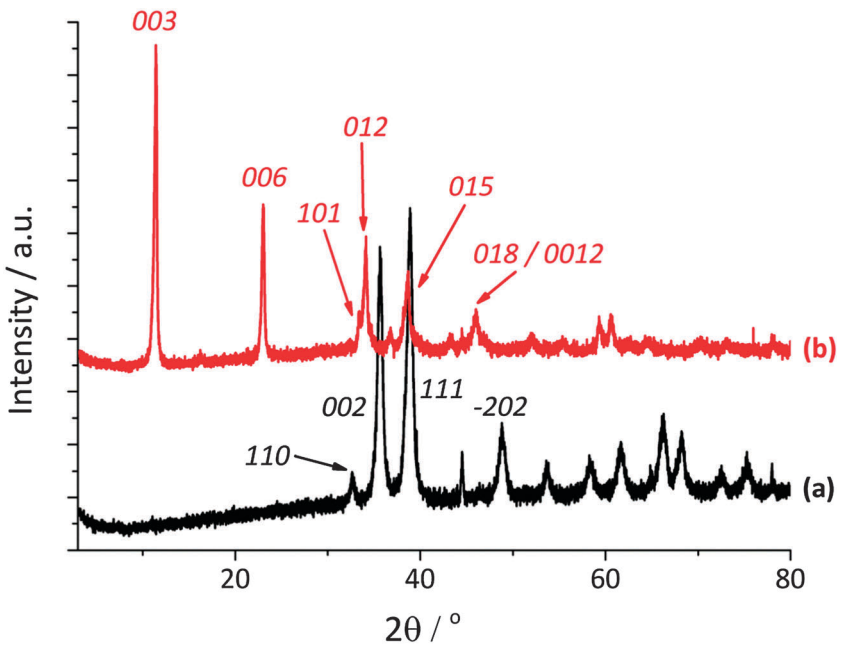

Fig. 11 X-ray diffraction patterns of (a) CuO and (b) Cu_2Cr–Cl.

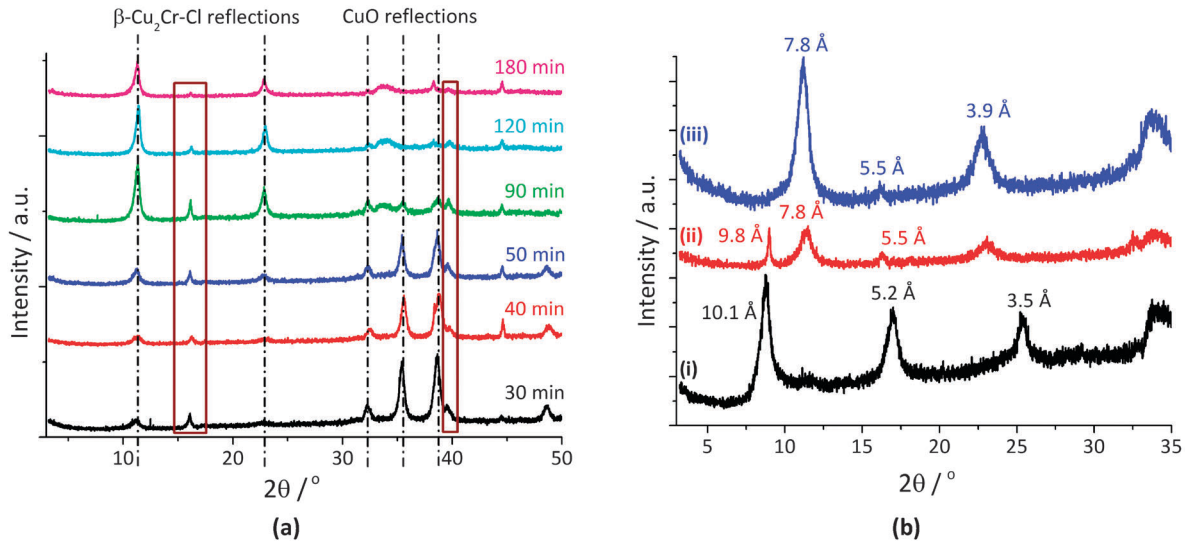

Fig. 12 (a) X-ray diffraction patterns of the quenched products recovered at various timepoints during the formation of Cu_2Cr–Cl, showing the presence of reflections from β-Cu_2Cr–Cl, CuO and a third phase (boxed); (b) diffraction patterns of (i) a wet product, showing a more hydrated α-phase with an interlayer spacing of *ca.* 10–10.5 Å, (ii) a partially dry material where both the α and β phases can be seen, and (iii) the dried β-phase product.

may proceed *via* initial hydration of the CuO matrix. It may be that a slightly hydrated form of $Cu(OH)_2$ forms: the material has a one-dimensional structure, and thus a small degree of hydration would cause the basal reflections to move to higher *d*-spacing. The observation of the $Cu(OH)_2$ phase in the quenched samples is in good agreement with the *in situ* data obtained with low concentrations of Cr, where this phase also appears to be present.

The α-phase could not be observed in the patterns of the thoroughly dried aliquots which contained only reflections from β-Cu_2Cr–Cl, suggesting that the α-phase may be a more hydrated form of the LDH. However, if the solid material from the reaction is recovered, filtered, and then a XRD pattern rapidly recorded while it is still damp, the higher *d*-spacing α-phase is clearly visible. The phase still exists even after two weeks of reaction at room temperature. XRD patterns depicting these observations are given in Fig. 12(b). It should be noted that the *006* of the more hydrated α-phase overlaps with the most intense reflection of the proposed $Cu(OH)_2$ intermediate; this makes the two phases impossible to resolve *in situ,* and only once the material has dried can we clearly see the copper hydroxide phase. Once dehydration to the β-Cu_2Cr–Cl material has occurred, it appears rehydration to the α-phase is not possible: attempts to achieve this by making slurries resulted in only β-Cu_2Cr–Cl being observed.

IR spectroscopy. IR data are shown in Fig. 13. In the very early stage of the reaction, no distinct absorbance peaks can be seen in the range 750–4000 cm^{-1} (Cu–O stretches and bends

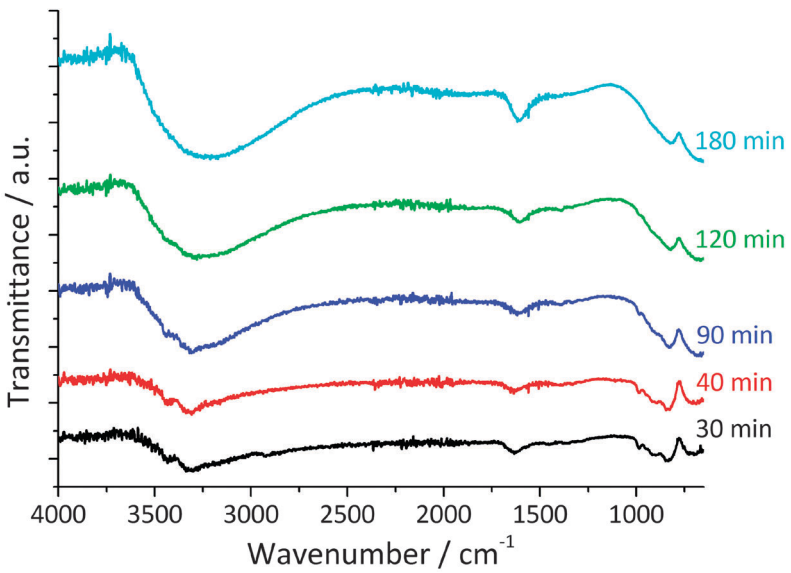

Fig. 13 IR spectra recorded from quenched samples during the formation of Cu_2Cr–Cl with 0.25 M $CrCl_3{\cdot}6H_2O$ at RT.

occur below 750 cm^{-1}). After *ca.* 30 minutes, a broad band begins to emerge centred around 3300 cm^{-1}, corresponding to H-bonded OH stretching. A second peak develops at approximately 1610–1620 cm^{-1}: this is the δ-bend of interlayer water molecules. These peaks, together with broad LDH M–OH vibrations below 1000 cm^{-1},[21,50] increase in intensity until around 180 min.

Scanning electron microscopy. Scanning electron microscopy (SEM) was used to assess the morphology of the particles during reaction: the results are given in Fig. 14. After 30 minutes of reaction (Fig. 14(a)), the solid material isolated comprised 100–200 nm particles, with a few platelets also visible. After 90 minutes, corrugated platelets around 500–1000 nm in size (see Fig. 14(b)) are observed. In addition to the platelets, some small irregularly sized particles are present (inset of Fig. 14(b). After 180 minutes or more of reaction, the solid product comprises solely platelets (see Fig. 14(c)).

Atomic emission spectroscopy. The variation in the metal ion content of the reaction solution as a function of time is depicted in Fig. 15(a). With increasing time, the amount of Cr in solution declines, and the amount of Cu in solution increases. The rates of these two processes are approximately the same: that is, Cu is freed from the CuO starting material into solution at *ca.* the same rate that Cr is absorbed into the solid matrix. This process appears to mirror changes in the XRD patterns and IR spectra with time. Approximately one third of the total Cu content of CuO is freed into solution, showing that dissolution of the starting material plays a significant role in the reaction mechanism. The amount of Cu released is the same as the amount of Cr taken up: thus, for every Cu ion released into solution, one Cr ion is taken up into the solid matrix. In ppm terms, the total Cu concentration in the system is *ca.* 31 600 ppm and that of Cr 13 500 ppm.

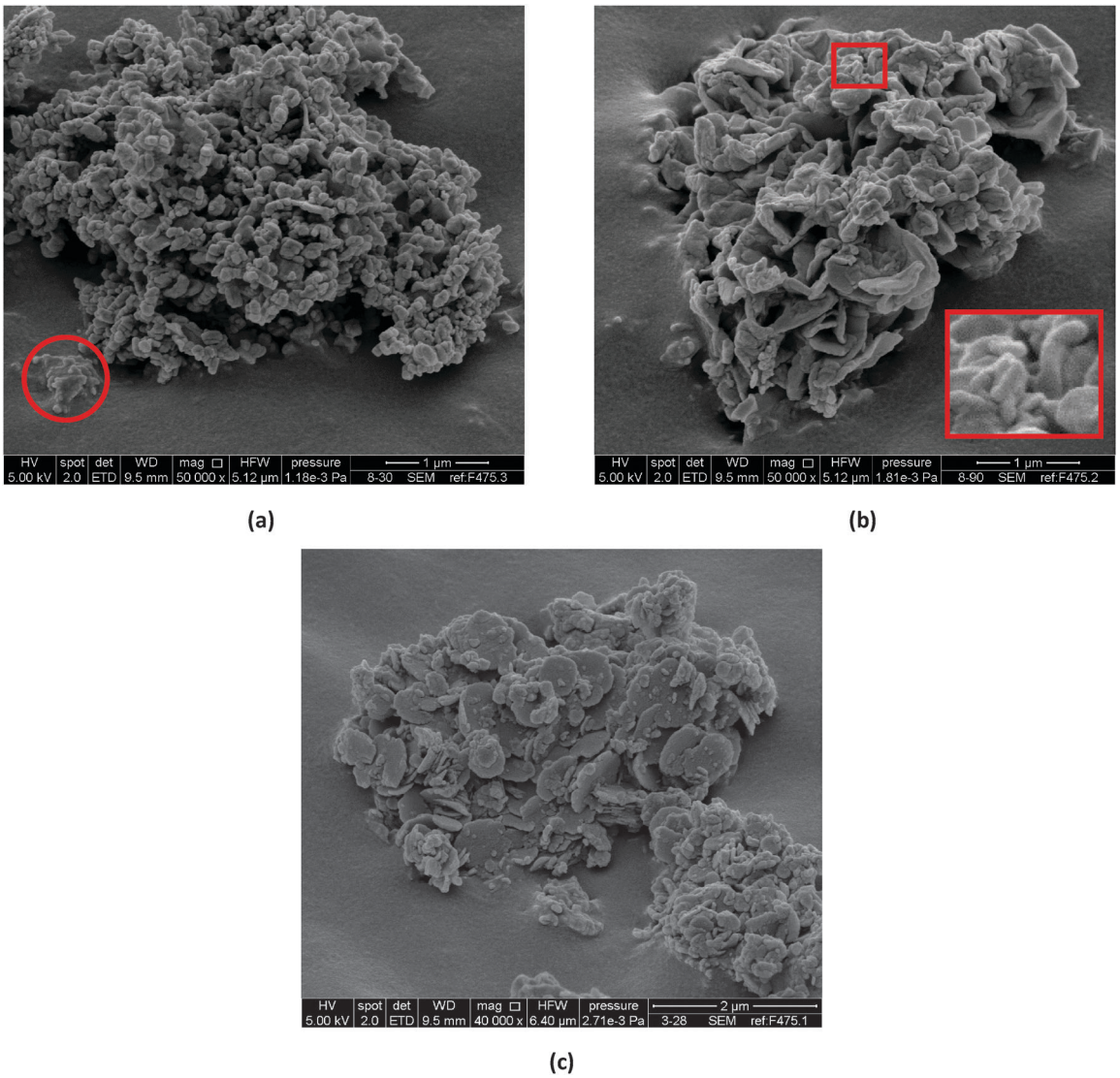

Fig. 14 SEM images of the solid products isolated after (a) 30 min; (b) 90 min; and, (c) 7 days of reaction between CuO and 0.25 M $CrCl_3{\cdot}6H_2O$ at room temperature. The feature circled in part (a) shows a small number of platelets which have formed; the inset in (b) is an enlargement of the red box, and illustrates the presence of irregularly shaped particles in addition to platelets.

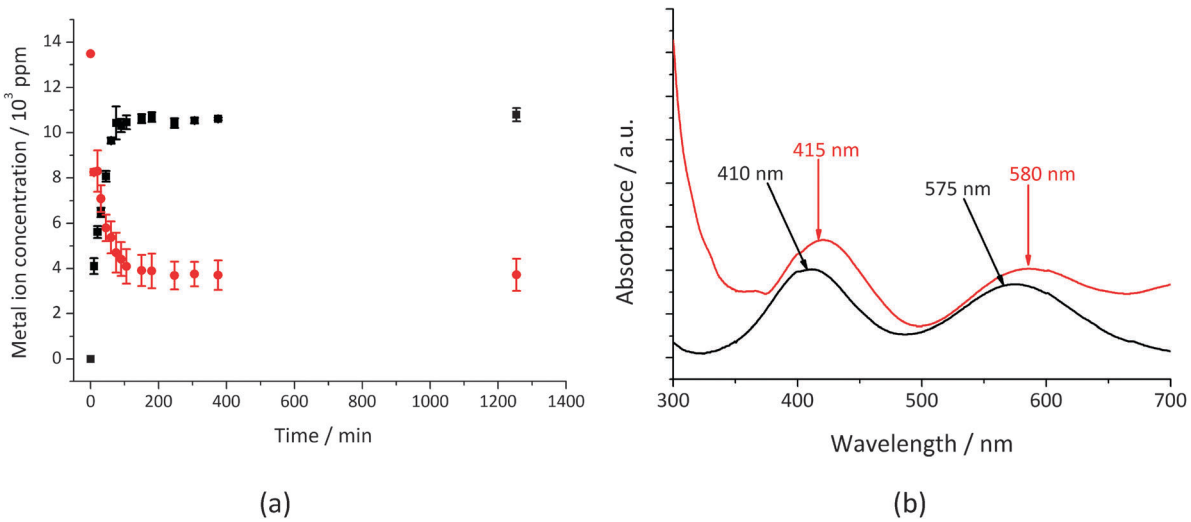

Fig. 15 Experimental data collected on the liquid phase during the formation of the Cu_2Cr–Cl LDH at room temperature. (a) Concentrations of Cu (■) and Cr (●) in solution as a function of reaction time, as determined by MP-AES. The reaction was monitored out to 10 000 min, but almost no further change was seen after 1250 min, and the later data are hence omitted for clarity. (b) UV spectra of freshly prepared $[Cr(OH)_6]^{3+}$ (—) and the solution recovered from the Cu_2Cr–Cl synthesis after one week (—).

Around 10 500 ppm of Cu is freed from the solid material into solution, and *ca.* 10 000 ppm of Cr taken up. This is consistent with the formation of a solid material of nominal formula $[Cu_2Cr(OH)_6]Cl{\cdot}yH_2O$, with a 2 : 1 ratio of Cu : Cr.

UV-visible spectroscopy. The nature of the species in solution were further probed by UV-vis spectroscopy. The spectra observed in the very early stages of the reaction ($t < 30$ min) are similar to the spectrum of $[Cr(OH_2)_6]^{3+}$. However, detailed examination of the spectra revealed that there is a small difference in peak position between the samples removed from the Cu_2Cr–Cl synthesis and freshly-made $[Cr(OH_2)_6]^{3+}$ (Fig. 15(b)). The spectrum of the latter displays the $^4A_{2g} \rightarrow {}^4T_{1g}$ and $^4A_{2g} \rightarrow {}^4T_{2g}$ transitions at 410 nm and 575 nm respectively, with an intensity ratio of $I_{410}/I_{575} = 1.18$, in excellent agreement with the literature values.[51] However, for the aliquots removed from the reaction gel, the $^4A_{2g} \rightarrow {}^4T_{1g}$ transition can be observed at 415 nm, and the $^4A_{2g} \rightarrow {}^4T_{2g}$ transition is found at 580 nm. The ratio $I_{415}/I_{580} \approx 1.25$. These values are close to the reported values for the oligomeric $[Cr_2(OH)_2(H_2O)_8]^{4+}$ species.[51] This dimer has previously been reported over the pH range 2.8–5.0, the same range as seen in these experiments. The formation of such oligomeric species *en route* to LDH formation has previously been observed by Briois and co-workers.[31]

The Cr^{3+} $^4A_{2g} \rightarrow {}^4T_{1g}$ and $^4A_{2g} \rightarrow {}^4T_{2g}$ transitions do not change wavelength during the course of the reaction and the ratio of I_{415}/I_{580} also remains virtually constant, suggesting that the same Cr-containing species remain in solution throughout. However, with increasing reaction time, these peaks decline in intensity and a new, broad, peak centred at 810 nm grows into the spectrum. This is the $^2E_g \rightarrow {}^2T_{2g}$ transition of the $[Cu(OH_2)_6]^{2+}$ ion, with the broadness of the peak being a result of Jahn–Teller distortions in the d^9 Cu^{2+} ion. In this case, the peak observed in solution is at the same wavenumber as the freshly made $[Cu(OH_2)_6]^{2+}$ standard solution.

The λ_{max} absorbances of the Cr^{3+} and Cu^{2+} ions were used to follow the change in solution metal ion concentrations: the results of this analysis can be found in the ESI,† Fig. S1. These data are in excellent agreement with the results from AES, with around 70% of the initial Cr content in solution taken up into the LDH. From the concentrations observed in solution, it is possible to estimate the metal ratio in the LDH as *ca.* 2 : 1 Cu : Cr, confirming the results from atomic emission spectroscopy (AES).

Discussion

From all the data collected both *in situ* and *ex situ,* it is possible to gain significant insight into the reaction mechanism. It appears that dissolution of the CuO starting material is a key facet of the reaction process, which cannot therefore be described as topotactic. Around one third of the Cu in the oxide is released into solution, and for each Cu ion released it appears that one Cr ion is incorporated. As the reaction proceeds, increasing amounts of hydroxide and water units are observed in the solid material. There appear to be two distinct intermediate phases in the reaction system. These comprise a more hydrated (α) form of the Cu_2Cr–Cl LDH, with a *d*-spacing around 10.5 Å (*cf.* 7.75 Å for the dry β-Cu_2Cr–Cl), and what is believed to be $Cu(OH)_2$. On the basis of this information, it is possible to postulate an outline mechanism for the formation of the LDH. This is illustrated in Fig. 16. CuO may be regarded as a consisting of 1D chains of edge-sharing CuO_4 squares, with pairs of chains being connected at every vertex through an additional Cu ion (see Fig. 16) to form a 3D matrix. It is proposed that the first stage of reaction involves the hydrolysis of these linkages, with H_3O^+ ions present in the acidic medium protonating the vertex oxygens, and the linking Cu being released into solution as $[Cu(OH_2)_6]^{2+}$.

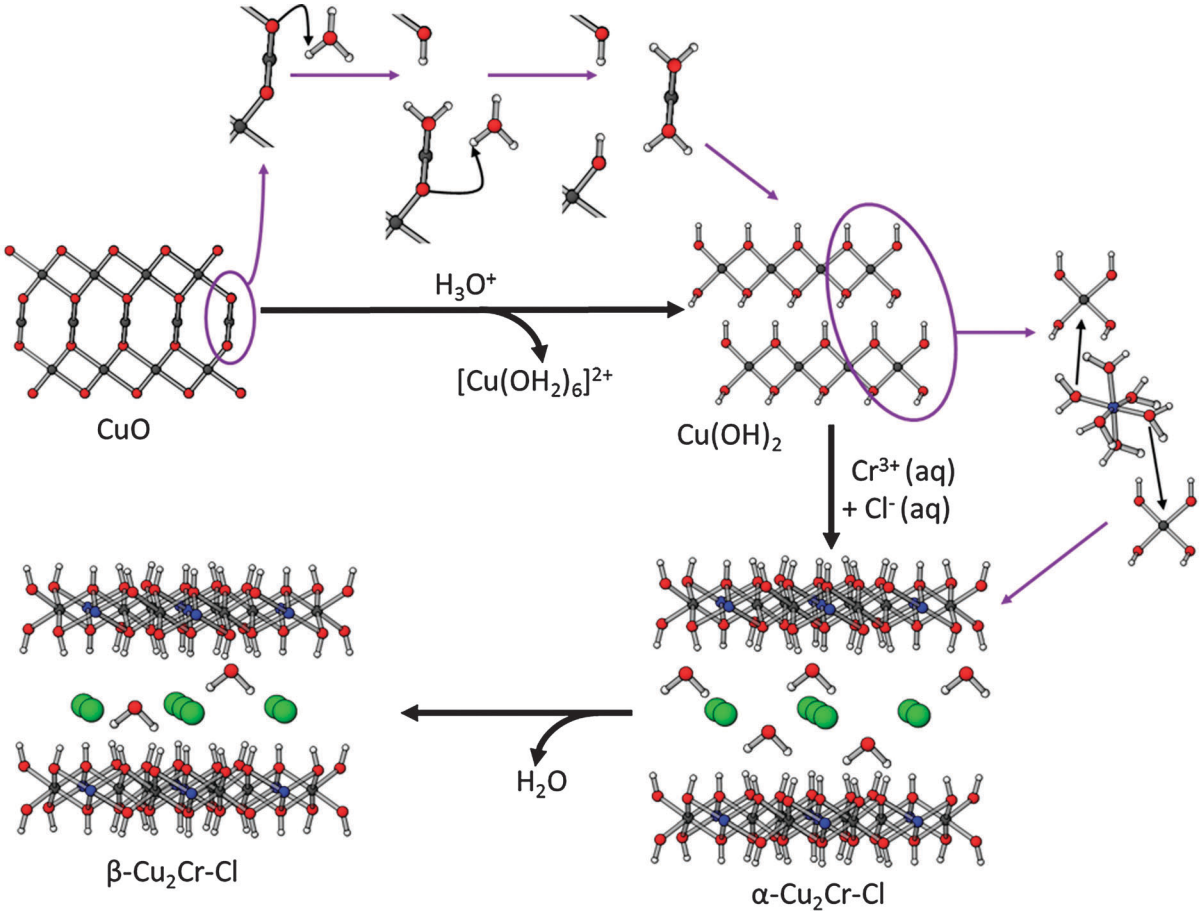

Fig. 16 Schematic illustrating the proposed mechanism of formation of Cu_2Cr–Cl from CuO and aqueous Cr^{3+}.

This is consistent with the results of AES (such hydrolysis releases one third of the total number of copper ions in the CuO, as seen by AES) and UV-visible spectroscopy, which shows Cu being released into the reaction medium as its hexaaqua complex. This yields $Cu(OH)_2$, a 1D material containing edge-sharing $Cu(OH)_4$ squares. The formation of this material is evidenced by XRD data, and is also supported by the SEM images (which contain irregular 1D-like particles at intermediate reaction times) together with the increase in OH content shown in IR spectroscopy. Next, the unsaturated Cu^{2+} ions in the chains increase their coordination number from 4 to 6 by condensing with aqueous Cr^{3+} species. Each Cr^{3+} ion can join with two $Cu(OH)_4$ squares, and in this way two chains are connected together. This must happen twice for every Cu in the chains, linking them together in two dimensions to form infinite planes. The introduction of Cr^{3+} into the solid material causes the layers to bear a positive charge, and so Cl^- anions are also incorporated between the layers, resulting in platelet materials. Initially, a more hydrated phase forms (the α-phase), before water is extruded to form the final β-Cu_2Cr–Cl product. These hypotheses are again supported by both the *in situ* and *ex situ* XRD analysis.

The values of the exponent n calculated from Avrami–Erofe'ev analysis are also consistent with this mechanism – it is generally seen that $1.5 < n < 2.5$, consistent with 3D diffusion control following deceleratory nucleation. If the nucleation sites are considered to be the Cu atoms linking the CuO_2 chains in the CuO starting material, then at the start of reaction there will be s nucleation sites available. Assuming all these are identical, the probability of reaction occurring at every site is the same (p), and the initial nucleation rate is ps. As the reaction proceeds, some of the nucleation sites q will have reacted, leaving s–q sites, and hence the nucleation rate is reduced to $(s–q)p$: deceleratory nucleation. The $Cu(OH)_2$ chains must then be condensed together in two dimensions, and stacked in the third dimension, resulting in a 3D process overall.

At elevated temperatures, the whole reaction is very rapid, with the intermediate phases too transient to be clearly observed, but at room temperature both $Cu(OH)_2$ and α-Cu_2Cr–Cl may be observed. Additional credence is given to the proposed mechanism by the concentration variation experiments: when the reaction is undertaken at room temperature with a reduced concentration of Cr^{3+}, the products of the reaction are observed to be β-Cu_2Cr–Cl and $Cu(OH)_2$. It is presumed that the reduced amount of Cr available for reaction means that although CuO hydrolysis can occur, there is insufficient Cr present to convert all of the $Cu(OH)_2$ produced

into the Cu_2Cr–Cl material, and hence considerable $Cu(OH)_2$ remains at the end of the reaction.

It should be noted that this proposed mechanism is likely to be over-simplified. Although the mechanism is shown for simplicity as a sequential step-wise process in Fig. 16, the *in situ* data show that the CuO starting material does not completely dissolve before LDH formation begins, and hence the various processes must be happening concomitantly. In addition, this reaction is a complex heterogeneous solid–solution transformation, and much of it is expected to occur in the solid–solution interface, where a number of complex equilibria will be operational. There are therefore other reaction pathways which may be involved in the transformation.

Conclusions

The formation of the Cu_2Cr–Cl LDH from CuO and $CrCl_3{\cdot}6H_2O$ in water was explored using *in situ* X-ray diffraction and *ex situ* analyses. It is proposed that the reaction occurs in three steps, with initial formation of $Cu(OH)_2$ chains *via* hydrolysis of CuO followed by subsequent condensation of these chains with aqueous Cr^{3+} species, Cl^- ions and water modules to give a more hydrated form of the LDH (α-Cu_2Cr–Cl). This material then extrudes some water to form the final β-Cu_2Cr–Cl product. This mechanism is consistent with all observed *in situ* measurements, and with *ex situ* analyses performed by X-ray diffraction, IR spectroscopy, scanning electron microscopy, UV-visible spectroscopy, and atomic emission spectroscopy.

Acknowledgements

The authors gratefully thank the following: Diamond Light Source for access to Beamline I12 (EE7782-1); the Deutsches Elecktronen-Synchrotron for the provision of beamtime on DORIS (I-20110410 EC); Dr Joern Donges and Dr Andre Rothkirch (DESY) for their assistance during experiments on F3; Dr Christina Reinhard (Diamond) for help and support with experiments on Beamline I12 of the Diamond Light Source; Professor Dermot O'Hare and Mr Saul Moorhouse (University of Oxford) for access to ODISC; Mr David McCarthy (UCL School of Pharmacy) for SEM measurements; Dr Andew Jupe (University of Oxford) for assistance with EDXRD data analysis; and, Dr Dominic Spillane (London Metropolitan University) for help with AES data collection. The research leading to these results has received funding from the European Community's Seventh Framework Programme (FP7/2007-2013) under grant agreement no. 312284.

References

1 G. R. Williams and D. O'Hare, *J. Mater. Chem.*, 2006, **16**, 3065.
2 A. I. Khan and D. O'Hare, *J. Mater. Chem.*, 2002, **12**, 3191.
3 *Layered Double Hydroxides: Present and Future*, ed. V. Rives, Nova Science Publishers, Hauppauge, NY, USA, 2001.
4 A. V. Besserguenev, A. M. Fogg, R. J. Francis, S. J. Price, D. O'Hare, V. P. Isupov and B. P. Tolochko, *Chem. Mater.*, 1997, **9**, 241.
5 A. M. Fogg, A. J. Freij and G. M. Parkinson, *Chem. Mater.*, 2002, **14**, 232.
6 J. He, M. Wei, B. Li, D. G. Evans and X. Duan, in *Layered Double Hydroxides*, ed. D. G. Evans and X. Duan, Springer, Berlin, 2006, vol. 119, p. 89.
7 M. Meyn, K. Beneke and G. Lagaly, *Inorg. Chem.*, 1990, **29**, 5201.
8 V. R. L. Constantino and T. J. Pinnavaia, *Inorg. Chem.*, 1995, **34**, 883.
9 E. Gardner, K. M. Huntoon and T. J. Pinnavaia, *Adv. Mater.*, 2001, **13**, 1263.
10 G. R. Williams and D. O'Hare, *J. Phys. Chem. B*, 2006, **110**, 10619.
11 A. M. Fogg, A. J. Freij and G. M. Parkinson, *Chem. Mater.*, 2002, **14**, 232.
12 H.-P. Boehm, J. Steinle and C. Vieweger, *Angew. Chem., Int. Ed. Engl.*, 1977, **16**, 265.
13 K. El Malki, A. De Roy and J. P. Besse, *Eur. J. Solid State Inorg. Chem.*, 1989, **26**, 339.
14 E. Zhouri and A. El Habji, *Ann. Chim. Sci. Mat.*, 1999, **24**, 57.
15 L. Bigey, C. Depege, A. De Roy and J. P. Besse, *J. Phys. IV*, 1997, **7**, 949.
16 C. Taviot-Gueho, F. Leroux, C. Payen and J. P. Besse, *Appl. Clay Sci.*, 2005, **28**, 111.
17 H. Roussel, V. Briois, E. Elkaim, A. De Roy and J. P. Besse, *J. Phys. Chem. B*, 2000, **104**, 5915.
18 C. Depege, C. Forano, A. de Roy and J. P. Besse, *Mol. Cryst. Liq. Cryst. Sci. Technol., Sect. A*, 1994, **244**, 161.
19 C. Forano, A. de Roy, C. Depege, M. Khaldi, F. Z. El Metoui and J. P. Besse, *Chem. Ind.*, 1997, **69**, 607.
20 S. Fleutot, J. C. Dupin, G. Renaudin and H. Martinez, *Phys. Chem. Chem. Phys.*, 2011, **13**, 17564.
21 V. Prevot, C. Forano and J. P. Besse, *Appl. Clay Sci.*, 2001, **18**, 3.
22 G. R. Williams, N. H. Rees and D. O'Hare, *Solid State Sci.*, 2009, **11**, 1229.
23 V. Prevot, C. Forano and J. P. Besse, *J. Solid State Chem.*, 2000, **153**, 301.
24 E. M. Moujahid, F. Leroux, M. Dubois and J. P. Besse, *C. R. Chim.*, 2003, **6**, 259.
25 E. M. Moujahid, M. Dubois, J. P. Besse and F. Leroux, *Chem. Mater.*, 2005, **17**, 373.
26 L. Tian, Y. Zhao, S. He, M. Wei and X. Duan, *Chem. Eng. J.*, 2012, **184**, 261.
27 A. M. Fogg and D. O'Hare, *Chem. Mater.*, 1999, **11**, 1771.
28 X. P. Xu and G. Q. Lu, *Chem. Mater.*, 2005, **17**, 1055.
29 S. Mitchell, T. Biswick, W. Jones, G. Williams and D. O'Hare, *Green Chem.*, 2007, **9**, 373.
30 Y. Yang, Z. Zhao, Y. Zhu and F. Zhang, *Chem. Mater.*, 2012, **24**, 81.
31 H. Roussel, V. Briois, E. Elkaim, A. De Roy, J. P. Besse and J. P. Jolivet, *Chem. Mater.*, 2001, **13**, 329.
32 R. P. Grosso Jr., S. L. Suib, R. S. Weber and P. F. Schubert, *Chem. Mater.*, 1992, **4**, 9228.
33 A. Michalik, A. Pacula, E. M. Serwicka, K. Bahranowski, A. Gawel, A. Dziembaj and E. Bielanska, *J. Pol. Chem. Soc.*, 2004, **78**, 1997.

34 J. S. O. Evans, R. J. Francis, D. O'Hare, S. J. Price, S. M. Clarke, J. Flaherty, J. Gordon, A. Nield and C. C. Tang, *Rev. Sci. Instrum.*, 1994, **66**, 2442.
35 http://www.diamond.ac.uk/Home/Beamlines/I12.html.
36 S. J. Moorhouse, N. Vranjes, A. Jupe, M. Drakopoulos and D. O'Hare, *Rev. Sci. Instrum.*, 2012, **83**, 084101.
37 A. P. Hammersley, *ESRF Internal Report*, 1998, ESRF98-HA01T, FIT2D V9.129 Reference Manual V123.121.
38 A. P. Hammersley, S. O. Svensson, M. Hanfland, A. N. Fitch and D. Haeusermann, *High Pressure Res.*, 1996, **14**, 235.
39 J. C. Burley, D. O'Hare and G. R. WIlliams, *Anal. Methods*, 2011, **3**, 814.
40 G. R. Williams, J. Crowder, J. C. Burley and A. M. Fogg, *J. Mater. Chem.*, 2012, **2012**, 22.
41 *R: a Language and Environment for Statistical Computing.* R Core Team, R Foundation for Statistical Computing, Vienna, Austria 2012, www.R-project.org.
42 V. Prevot, C. Forano and J. P. Besse, *J. Solid State Chem.*, 2000, **153**, 301.
43 D. O'Hare, J. S. O. Evans, A. Fogg and S. O'Brien, *Polyhedron*, 2000, **19**, 297.
44 M. Avrami, *J. Phys. Chem.*, 1941, **9**, 177.
45 M. Avrami, *J. Phys. Chem.*, 1940, **8**, 212.
46 S. F. Hulbert, *J. Br. Ceram. Soc.*, 1969, **6**, 11.
47 M. J. Pilling and P. W. Seakins, *Reaction Kinetics*, Oxford University Press, Oxford, 1995.
48 S. Asbrink and L. Norrby, *Acta Crystallogr., Sect. B: Struct. Crystallogr. Cryst. Chem.*, 1970, **26**, 8.
49 F. Leroux, P. Aranda, J. P. Besse and E. Ruiz-Hitxky, *Eur. J. Inorg. Chem.*, 2003, 1242.
50 M. C. Richardson and P. S. Braterman, *J. Phys. Chem. C*, 2007, **111**, 4209.
51 H. Stuenzi and W. Marty, *Inorg. Chem.*, 1983, **22**, 2145.

